Two-fluid theory of collisionless magnetic reconnection

D. Biskamp and E. Schwarz
Max-Planck-Institut für Plasmaphysik, 85748 Garching, Germany

J. F. Drake
Institute for Plasma Research, University of Maryland, College Park, Maryland 20742

(Received 5 September 1996; accepted 16 January 1997)

Theoretical studies of collisionless reconnection in the framework of two-fluid theory are presented. In the high-β case ($\beta \gtrsim 1$) reconnection is controlled by the whistler mode, leading to decoupling of ions from electrons on scales $< c/\omega_{pi}$. Though reconnection requires electron inertia, the reconnection rate is independent thereof, controlled only by ion inertia. Reconnection is hence much faster than in the absence of the Hall term. In the opposite limit of small β the strong axial field suppresses the whistler mode. Hence ions have to follow the electrons in the narrow reconnection layer $\delta \sim c/\omega_{pe}$, forming a macroscopic current sheet which strongly reduces the reconnection rate. Theoretical scaling laws are confirmed by numerical simulations. © *1997 American Institute of Physics.* [S1070-664X(97)03304-1]

I. INTRODUCTION

Observations in laboratory and space clearly indicate that fast magnetic reconnection processes occur in nearly collisionless plasmas. For instance, the time scales of the collapse phase in the so-called sawtooth oscillation, a relaxation oscillation in the core of a tokamak discharge, which necessarily involves reconnection, is much shorter than could be accounted for by the collisional effects in Ohm's law, resistivity and electron viscosity.[1] Even more stunning are various types of magnetic processes observed in the extraterrestrial environment, notably magnetospheric substorms, which seem to be caused by reconnection in the earth's magnetotail,[2] and solar flares, where reconnection occurs in the solar corona,[3] both plasmas being almost collisionless.

Theoretical analysis of collisionless plasma processes usually requires a kinetic model. This is obviously true, if particle distribution functions deviate strongly from Maxwellian, in particular developing long tails resulting from acceleration of particles to highly superthermal energies. But also for roughly isotropic distributions, kinetic effects may be important, if Larmor radii exceed typical gradient scales. If superthermal particles are negligible and the Larmor radii are sufficiently small, collisionless dynamics can be investigated approximately in the framework of fluid theory, which is much more convenient both analytically and in numerical simulations. A fluid description usually requires some dissipation, notably viscosity, to prevent solutions from becoming singular. There may be some doubt, whether such processes should then be called collisionless. Here we distinguish between collisional and quasi-collisionless processes on account of the dominant reconnection mechanism. While in the former case the dynamics, in particular the reconnection time scale, depends sensitively on the value of the dissipation coefficient, it is essentially independent thereof in the latter, where the role of dissipation is not basically different from the coarse-graining process required to introduce irreversibility and dissipation in the Vlasov theory.

Recently several theoretical and numerical studies indicate that the nondissipative terms in Ohm's law, electron inertia,[4,5] electron pressure,[6–8] and the Hall term,[9,10] which have usually been neglected in previous reconnection theories,[11] may give rise to rapid reconnection or speed up the reconnection process. In this paper we give a detailed picture of quasi-collisionless reconnection in high-β plasmas, which is dominated by the Hall term, and discuss the transition to the low-β case, where the effect of the Hall term is suppressed. In section II a set of fluid equations is introduced, which are solved in two-dimensional plane geometry. In section III the high-β case is treated, which is dominated by the whistler dynamics. In the region $|x| < c/\omega_{pi}$ around the X-point, where the ion motion can be neglected, we give a quasi-quantitative solution of the reconnection configuration. We find that the micro-current sheet at the X-point adjusts automatically to the outside flow, such that the reconnection rate E is independent of the electron parameters, c/ω_{pe} and electron viscosity. E depends only on ion inertia c/ω_{pi}. Numerical simulations show that this dependence is rather weak, hence reconnection is fast for $\beta \gtrsim 1$. In the low-β case, treated in section IV, the axial magnetic field suppresses the coupling to the whistler mode, which strongly reduces the reconnection efficiency. Section V summarizes the results and gives some comments concerning kinetic effects.

II. THE TWO-FLUID MODEL

The framework of a macroscopic theory of quasi-collisionless reconnection is the general two-fluid equations. It is, however, useful to introduce a number of restrictions, which simplify the equations considerably:

(a) Quasi-neutrality. We assume that the Debye length is smaller than all relevant spatial scales. Hence ion and electron densities are essentially equal $n_i = n_e = n$.

(b) Electron and ion pressure tensors are assumed isotropic described by scalar pressures p_e, p_i. This is, strictly speaking, not in the spirit of collisionless fluid theory such as the Chew-Goldberger-Low double adiabatic theory. Since, however, our interest is mainly in nearly

 1070-664X/97/4(4)/1002/8/$10.00

incompressible processes, details of the pressure behavior are not important. For the same reason a simple scalar heat conductivity is chosen.

(c) The average pressure and density profiles are assumed homogeneous. Thus diamagnetic effects are ruled out. Their effect is briefly discussed in section IV.

(d) The stress tensors $\boldsymbol{\pi}_{i,e}$ are reduced to scalar collisional viscosity terms. Since singularities tend to arise primarily in the velocity gradients, electron viscosity is more important than resistivity, which is hence neglected. We also include the nondissipative gyroviscosity for the ions thus accounting in a crude way for finite Larmor radius effects.

The electric field is determined by Ohm's law,

$$\mathbf{E}=-\frac{1}{c}\mathbf{v}_e\times\mathbf{B}-\frac{1}{ne}\nabla p_e-\frac{m_e}{en}(\partial_t n\mathbf{v}_e+\nabla\cdot\mathbf{v}_e\mathbf{v}_e n)-\mu_e\frac{m_e}{e}\nabla^2\mathbf{v}_e. \tag{1}$$

The ion equation of motion is

$$m_i(\partial_t n\mathbf{v}_i+\nabla\cdot\mathbf{v}_i\mathbf{v}_i n)-en\left(\mathbf{E}+\frac{\mathbf{v}_i}{c}\times\mathbf{B}\right)+\nabla p_i=\mu_i m_i n\nabla^2\mathbf{v}_i-\mu_0 m_i\mathbf{b}\times\nabla^2\mathbf{v}_i. \tag{2}$$

μ_e,μ_i are the kinematic viscosities, and the gyroviscosity is $\mu_0=cT_i/eB$, $\mathbf{b}=\mathbf{B}/B$. The pressure equations are simply:

$$\partial_t p_{e,i}+\mathbf{v}_{e,i}\cdot\nabla p_{e,i}+\gamma p_{e,i}\nabla\cdot\mathbf{v}_{e,i}=\kappa\nabla^2 p_{e,i}, \tag{3}$$

where κ is a small phenomenological scalar heat diffusivity. The magnetic field follows from Faraday's law

$$\partial_t\mathbf{B}=-c\nabla\times\mathbf{E}, \tag{4}$$

and Ampère's law connects the fluid velocities to the magnetic field

$$en(\mathbf{v}_i-\mathbf{v}_e)=\mathbf{j}=\frac{c}{4\pi}\nabla\times\mathbf{B}. \tag{5}$$

The electric field is eliminated from (2) and (4) by inserting expression (1), and $\mathbf{v}_e$ is expressed by $\mathbf{v}_i$ and $\mathbf{j}$.

These equations are solved in two-dimensional (2D) plane geometry. Since we are mostly interested in the nearly incompressible case, we assume that the density is homogeneous $n=n_0=$ const. The magnetic field is written in the form

$$\mathbf{B}=\mathbf{e}_z\times\nabla\psi+\mathbf{e}_z(B_{z0}+b), \tag{6}$$

splitting the axial component into a background field B_{z0} and a fluctuating part, $\langle b\rangle=0$. The current density then becomes

$$\mathbf{j}=\mathbf{j}_\perp+\mathbf{e}_z j_z=\frac{c}{4\pi}(\nabla b\times\mathbf{e}_z+\mathbf{e}_z\nabla^2\psi). \tag{7}$$

While in the high-β case $\mathbf{v}_e$ in the electron inertia term could well be approximated by $-\mathbf{j}/ne$, in the low-β case, where $B_{z0}\gg B_\perp$, we find $\mathbf{v}_{e\perp}\simeq\mathbf{v}_{i\perp}\gg\mathbf{j}_\perp/ne$ even in the diffusion layer. Hence we do not make this approximation. To write the basic equations in nondimensional form, we introduce the following normalizations. Since the whistler mode plays a particular role in these studies, we use the whistler time $\tau_w=L^2/d_e^2\Omega_e$ as time unit instead of the Alfvén time $\tau_A=L/v_A$, where L is some characteristic spatial scale and B_0 entering Ω_e and v_A a characteristic poloidal field intensity. In these units the equations read:

$$\partial_t(\psi+d_e^2 v_{ez})+\mathbf{v}_e\cdot\nabla(\psi+d_e^2 v_{ez})=\nu_e\nabla^2 v_{ez}, \tag{8}$$

$$\partial_t(b-d_e^2\omega_e)+\mathbf{v}_e\cdot\nabla b+(B_{z0}+b)\nabla\cdot\mathbf{v}_e-\mathbf{B}\cdot\nabla v_{ez}-d_e^2(\nabla\times\nabla\cdot\mathbf{v}_e\mathbf{v}_e)\cdot\mathbf{e}_z=-\nu_e\nabla^2\omega_e, \tag{9}$$

$$d_i^2(\partial_t\mathbf{v}_{i\perp}+\nabla\cdot\mathbf{v}_{i\perp}\mathbf{v}_{i\perp})+d_e^2(\partial_t\mathbf{v}_{e\perp}+\nabla\cdot\mathbf{v}_{e\perp}\mathbf{v}_{e\perp})+\nabla(p_i+p_e)+(B_{z0}+b)\nabla b+\nabla^2\psi\nabla\psi=\nu_i\nabla^2\mathbf{v}_{i\perp}+\nu_e\nabla^2\mathbf{v}_{i\perp}-\nu_0\mathbf{e}_z\times\nabla^2\mathbf{v}_{i\perp}, \tag{10}$$

$$d_i^2(\partial_t v_{iz}+\nabla\cdot\mathbf{v}_{i\perp}v_{iz})+d_e^2(\partial_t v_{ez}+\nabla\cdot\mathbf{v}_{e\perp}v_{ez})-\mathbf{B}\cdot\nabla b=\nu_i\nabla^2 v_{iz}+\nu_e\nabla^2 v_{ez}, \tag{11}$$

$$\partial_t p_i+\mathbf{v}_i\cdot\nabla p_i+\gamma p_i\nabla\cdot\mathbf{v}_i=\kappa\nabla^2 p_i, \tag{12}$$

$$\partial_t p_e+\mathbf{v}_e\cdot\nabla p_e+\gamma p_e\nabla\cdot\mathbf{v}_e=\kappa\nabla^2 p_e, \tag{13}$$

where $\mathbf{v}_{e\perp}=\mathbf{v}_{i\perp}+\mathbf{e}_z\times\nabla b$, $v_{ez}=v_{iz}-\nabla^2\psi$, $d_{e,i}=c/\omega_{pe,i}L$, $\nu_e=\mu_e d_e^2,\nu_{i,0}=\mu_{i,0}d_i^2$. Since the collisional value of ν_e would be negligibly small, ν_e represents an effective viscosity due to a slight stochastic braiding of magnetic field lines. Here we consider ν_e,ν_i,ν_0 essentially as small phenomenological parameters, introduced to prevent solutions from becoming singular. For sufficiently small values the global dynamics is found to be independent thereof. Since $\nabla\cdot\mathbf{j}=0$, we have $\nabla\cdot\mathbf{v}_e=\nabla\cdot\mathbf{v}_i$ for constant n. It is interesting to note that when inserted in Faraday's law the electron pressure term in Ohm's law vanishes for constant density. Therefore in this framework we do not include the p_e effect considered in Refs. 6–8. Those papers consider only the parallel component of Ohm's law in a strongly magnetized system with $B_z\gg B_\perp$, which is briefly discussed in section IV. Equations (8)–(13) conserve momentum, but the enforced constancy of the density implies local sources and sinks of energy. Linearizing the equations about a static homogeneous equilibrium $p_{0i,e},B_{y0},B_{z0}$, neglecting dissipation and setting $\mathbf{v}_e=-\mathbf{j}$ in the electron inertia term yields the linear dispersion relation, which is still rather complicated in the general compressible case. Assuming incompressible motions $\nabla\cdot\mathbf{v}_{i,e}=0$ we obtain

$$\omega^2=\frac{k_\parallel^2k^2}{(1+k^2d_e^2)^2}+\frac{k_\parallel^2 d_i^{-2}}{1+k^2d_e^2}. \tag{14}$$

While for long wavelength $kd_i<1$ the last term dominates, representing the Alfvén wave, for smaller wavelength $kd_i>1$ one has a pure electron mode, the whistler: $\omega^2\simeq k_\parallel^2k^2$ and high group velocity $v_g\propto k$ for $kd_e<1$, $\omega^2\simeq k_\parallel^2/k^2d_e^4$ (or $\omega^2=\Omega_e^2k_\parallel^2/k^2$ in dimensional form) and small group velocity $v_g\simeq 0$ for $kd_e>1$. The whistler implies a coupling between poloidal and toroidal field perturbations,

$$b_{\mathbf{k}}=\pm k\psi_{\mathbf{k}}, \tag{15}$$

which is valid independently of the value of kd_e. We will see in section III that the whistler is the relevant mode for reconnection at sufficiently high plasma pressure, $\beta \gtrsim 1$. In the low-β case, $B_{z0} \gg B_\perp$, the $B_{z0}\nabla\cdot\mathbf{v}_e$ in Eq. (9) is not negligible even for nearly incompressible conditions. It leads to suppression of the whistler mode, leaving only the Alfvén wave also for $kd_i > 1$.

III. THE HIGH-β CASE

For high background pressure electron and ion motions are incompressible. Since the term $\gamma p_{i,e}\nabla\cdot\mathbf{v}_{i,e}$ in the pressure Eqs. (12), (13) must be finite, one has $\nabla\cdot\mathbf{v}_i = \nabla\cdot\mathbf{v}_e \simeq 0$. Assuming $\nabla\cdot\mathbf{v}_i = 0$ the pressure is no longer determined by Eq. (12) but from Poisson's equation obtained by taking the divergence of the equation of motion (10). Note that p does not affect the dynamics directly, it can be eliminated from Eq. (10) by applying the curl, which yields

$$d_i^2(\partial_t\omega_i + \mathbf{v}_i\cdot\nabla\omega_i) + d_e^2(\partial_t\omega_e + \mathbf{v}_e\cdot\nabla\omega_e) - \mathbf{B}\cdot\nabla j = \nu_i\nabla^2\omega_i + \nu_e\nabla^2\omega_e, \tag{16}$$

where $\omega_{i,e} = \nabla^2\varphi_{i,e}, \mathbf{v}_{i,e} = \mathbf{e}_z \times \nabla\varphi_{i,e}, \varphi_e = \varphi_i + b$. Equations (8), (11) for ψ, v_{iz} remain unchanged, while Eq. (9) can be written in the form

$$\partial_t(b - d_e^2\omega_e) + \mathbf{v}_e\cdot\nabla(b - d_e^2\omega_e) - \mathbf{B}\cdot\nabla v_{ez} = -\nu_e\nabla^2\omega_e. \tag{17}$$

If we assume that reconnection occurs in a localized region (X-point), the properties of the linear mode (14) suggest the existence of two different regions around this point: For scales exceeding $d_i, kd_i < 1$, the magnetohydrodynamic (MHD) picture applies, where electrons and ions move essentially together, $\mathbf{v}_i \simeq \mathbf{v}_e$; for smaller scales, $kd_i > 1$, the ions can no longer follow the electrons, $\mathbf{v}_i \simeq 0$, forming a static charge neutralizing background, while the dynamics is only determined by the electrons. This behavior is clearly seen in Figs. 1 and 2 illustrating a typical reconnection process, the merging of two flux bundles. (Details of the numerical procedure are discussed in section III B.) In Fig. 1 the flow patterns φ_e and φ_i show that when the ion flow is deviated into the outflow cone at some distance of order d_i, the electron flow is converging toward the X-point forming much smaller structures. This qualitative difference in the flow properties becomes more quantitative in Fig. 2, which shows the magnitude of the ion and electron velocities along the inflow directions, the diagonal across the X-point in Fig. 1: while $v_e \simeq v_i$ outside the ion inertial layer, ions are decelerated inside this layer, but electrons are accelerated, until finally they, too, are slowed down inside a much smaller layer of order d_e. Hence the small-scale reconnection dynamics inside the ion layer can be described ignoring the ion motion, $\mathbf{v}_i = 0$, $\mathbf{v}_e = -\mathbf{j} = -\nabla\times\mathbf{B}$. This approximation is called electron magnetohydrodynamics (EMHD), which has attracted considerable attention recently, being relevant in a variety of fast plasma processes, see e.g. Refs. 12–15. The 2D EMHD equations consist of Eqs. (8) and (17) with $b = \varphi_e$, $v_{ez} = -j = -\nabla^2\psi$,

$$\partial_t(\psi - d_e^2 j) + \mathbf{v}_e\cdot\nabla(\psi - d_e^2 j) = -\nu_e\nabla^2 j, \tag{18}$$

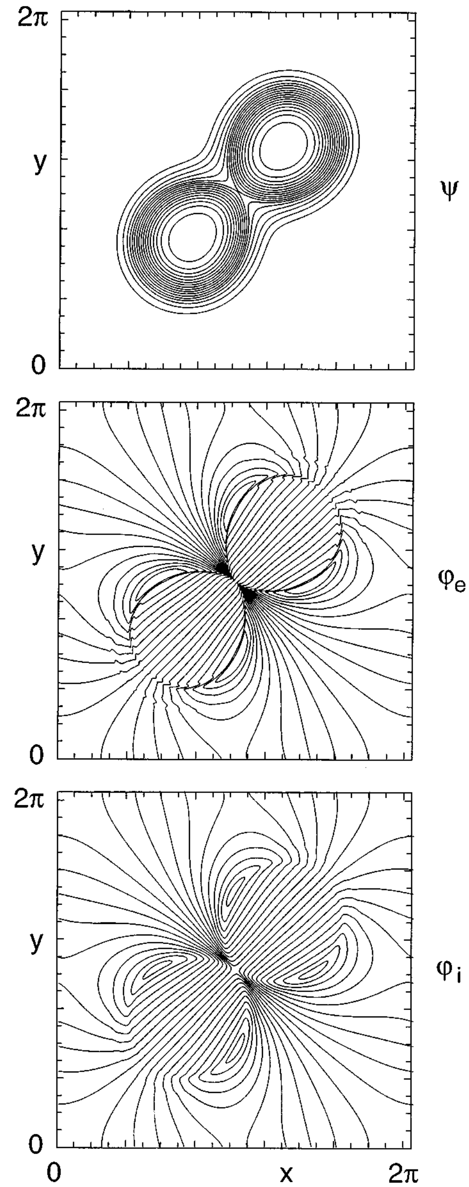

FIG. 1. Simulation of flux bundle coalescence with $d_i = 0.1$, $d_e = 0.015$, $\nu_i = 10^{-5}$, $\nu_e = 10^{-6}$.

$$\partial_t(\varphi_e - d_e^2\omega_e) + \mathbf{v}_e\cdot\nabla(\varphi_e - d_e^2\omega_e) + \mathbf{B}\cdot\nabla j = -\nu_e\nabla^2\omega_e. \tag{19}$$

A. Behavior in the reconnection region

In the region $|x| < d_i$ around the X-point we hence analyze the configuration in the EMHD framework assuming stationarity, which is valid as long as the flow is stable. Instability and resulting turbulence will be briefly discussed at the end of this subsection. We choose the coordinate system such that $\pm x$ defines the inflow and $\pm y$ the outflow directions. For $|x| \gg d_e$ the stationary equations are

$$E + \mathbf{v}_e\cdot\nabla\psi = 0, \tag{20}$$

$$\mathbf{B}\cdot\nabla\nabla^2\psi = 0, \tag{21}$$

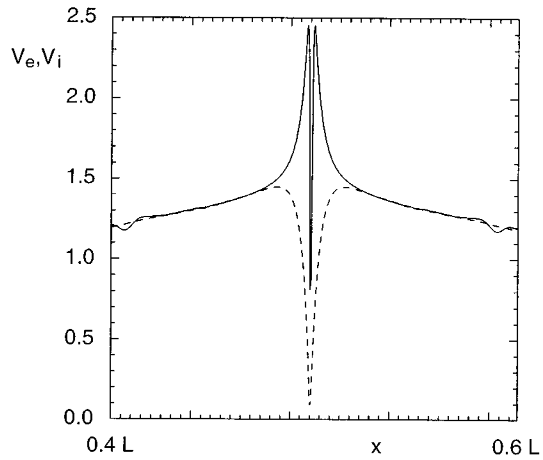

FIG. 2. Inflow velocities v_e (solid line) and v_i (dashed line) along the diagonal, from the simulation state shown in Fig. 1.

where $E=E_z=\partial_t\psi$ is the reconnection rate. These equations have the similarity solution:[16]

$$\psi=\frac{1}{2}(x^2-a^2y^2), \tag{22}$$

$$\varphi_e=\frac{E}{2a}\ln\left|\frac{x+ay}{x-ay}\right|. \tag{23}$$

The stream function φ_e implies, that the upstream flow converges toward the X-point and the downstream flow diverges away from it. Finite viscosity is only needed to smooth the flow singularity on the separatrix $x=\pm ay$. The scale parameter a allows a finite uniform current density, so that the separatrix branches may intersect at any angle.

We now show that the solution (22), (23) for $|x|>d_e$ can be matched to the electron inertia-dominated region $|x|<d_e$, where ψ and φ_e deviate from these expressions. In the limit of small viscosity the current layer, which forms in the inertia-dominated region, exhibits a complicated multiscale structure. In particular the current density $j=\nabla^2\psi$ develops a cusp-like singularity resulting from continuous acceleration at the X-point, the stagnation point of the flow.[4] The singularity is, however, only logarithmic,[5] so that it does not give a finite contribution to the integrated current. In the following order-of-magnitude discussion we will therefore neglect these substructures considering only average quantities.

The inertia-dominated region consists of a current layer of width δ and length Δ. From the convection term in Eq. (8) we see that inertia becomes important if

$$\partial_x\psi=B_y\sim d_e^2\partial_x j\sim d_e^2 B_y/\delta^2,$$

hence the layer width is

$$\delta\sim d_e. \tag{24}$$

Integrating the φ_e equation over a quadrant of the current layer region and using Gauss' theorem to transform the area integrals into line integrals over the boundary

$$d_e^2\oint dl v_{en}\omega_e=\oint dl B_n j,$$

we obtain the relation between the outflow velocity v and the axial current density:

$$v\sim j. \tag{25}$$

The equality of these flows results from the gyro-rotation of the out-of-plane current j into the outflow direction. The current layer can also be interpreted as a (finite amplitude) whistler perturbation satisfying Eq. (15) with $k\simeq k_x$, which is equivalent to Eq. (25). Integration of the continuity equation over a quadrant of the current layer connects the outflow velocity v to the inflow velocity u

$$u\Delta\sim v d_e. \tag{26}$$

Finally, to derive a relation for the layer length Δ we use the property that $F=\psi-d_e^2 j$, the electron canonical momentum in z direction, is constant along the current layer, $\partial_y F\simeq 0$, which is also seen in the numerical simulation (Fig. 4 below), $F|_{y=\Delta}=F|_{y=0}$. To determine the variation of ψ, we note that, while B_y is changed by the presence of the current sheet, B_x is not, as can be checked *a posteriori* using the resulting scaling laws for j and Δ. Hence $\partial_y B_x\sim 1$ leads to the relation

$$\psi(\Delta)\sim\Delta^2\sim d_e^2 j. \tag{27}$$

Let us write the resulting scaling laws for Δ, j, u in terms of the reconnection rate E. Using the relation $E\sim uB_y\sim ujd_e$ and Eqs. (24)–(27) one obtains

$$\Delta\sim(Ed_e^2)^{1/3}, \tag{28}$$

$$j\sim v\sim(E/d_e)^{2/3}, \tag{29}$$

$$u\sim(E/d_e)^{1/3}. \tag{30}$$

The length Δ of the layer given in Eq. (28) is simply the effective Larmor radius of electrons with velocity v in the magnetic field B_x. The scaling laws are consistent with the essential physics of the layer, the transformation of magnetic energy into streaming energy. The energy flux into the layer is mainly magnetic

$$uB_y^2\Delta\sim d_e\gg m_e u^3\Delta\sim d_e^{5/3}$$

with $m_e=d_e^2$ in our units. By contrast the energy flux out of the layer is mainly kinetic

$$m_e v^3\delta\sim d_e\gg vB_x^2\delta\sim d_e^{5/3},$$

using $B_x\sim\Delta$. We also see that the energy fluxes into and out of the layer are of the same order.

Relation (28) shows that Δ shrinks to zero for $d_e\to 0$. Since $B_y\sim jd_e\to 0$, there is no flux pile-up in front of the layer. The reconnection rate E is therefore independent of d_e (and ν_e) depending only on the global configuration, e.g. the free magnetic energy. This behavior differs strongly from reconnection in resistive MHD. Though outside the diffusion layer a solution similar to Eqs. (22), (23) is permitted (replacing the electron flow by the plasma flow), it cannot be matched to the diffusion layer, which in the MHD case is a current sheet of macroscopic length L. The essential differ-

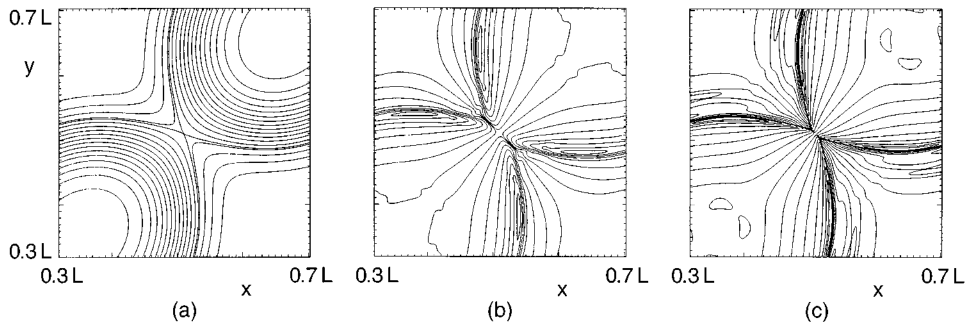

FIG. 3. Reconnection region from a simulation of flux bundle coalescence in the EMHD approximation. (a) ψ; (b) φ_e for $d_e = 0.06$; (c) φ_e for $d_e = 0.015$, (b) and (c) taken at the time; ψ is essentially identical in both cases.

ence is that in resistive MHD the outflow velocity v equals the upstream Alfvén velocity, which is finite, while the current density diverges for resistivity $\eta \rightarrow 0$. The reconnection rate depends strongly on $\eta, E \sim \eta^{1/2}$, for details see e.g. Ref. 17.

B. EMHD simulation results

The predictions of section III A are confirmed by numerical simulations. We consider the merging of two flux bundles located on the diagonal in a square box of edge size $L = 2\pi$ with periodic boundary conditions,

$$\psi = \exp\{-[(x-x_1)^2 + (y-y_1)^2]^2/4\} + \exp\{-[(x-x_2)^2 + (y-y_2)^2]/4\}, \tag{31}$$

where $x_1 = y_1 = \pi/2 + 0.6$, $x_2 = y_2 = 3\pi/2 - 0.6$. The rather square-shaped profiles are chosen to localize the flux tubes in order to avoid overlap between tubes in neighboring computational boxes thus minimizing the effect of the boundary conditions. We also add a low level random velocity field.

Equations (18), (19) are solved numerically using a standard pseudospectral method with dealiasing according to the 2/3 rule. The number of modes (more appropriately collocation points) N^2 is chosen suitably to provide adequate resolution, N varying between 256 and 2048.

A series of simulation runs have been performed with different values of the parameters d_e and ν_e. (In order to concentrate dissipation more strongly at small scales we use a higher order diffusion operator replacing $\nu_e \nabla^{(4)} \psi$, $\nu_e \nabla^{(4)} \varphi_e$ by $\nu_3 \nabla^{(6)} \psi$, $\nu_3 \nabla^{(6)} \varphi_e$, respectively.)

Figure 3 shows the region around the X-point for two different values of d_e. The inertia dominated region appears as a small layer of high velocity. [Note that the strong flows at the separatrix are a property of the similarity solution (23).] The layer shrinks in both length and width with decreasing d_e consistent with the scaling laws (24), (28).

In Fig. 4 a blowup of the reconnection region shown in Fig. 3 gives contours of ψ and $F = \psi - d_e^2 j$. This figure illustrates some important features of collisionless reconnection. Equation (18) implies that F is convected with the electron fluid motion. Since symmetry requires a stagnation point of the flow at the X-point, in the absence of dissipation F would simply pile up in front of the X-point and would remain topologically invariant. This pile up of F is clearly seen in Fig. 4(b) and is the reason F is nearly constant along the layer as discussed in section III A. However, the distortion of the contours of F in the outflow region clearly indicates that F is undergoing a topological change. This is a consequence of the finite dissipation in the system. The singular cusp-like structure of j near the X-point is reflected in a similar structure for F and allows F to change topology even in the limit of vanishingly small dissipation.

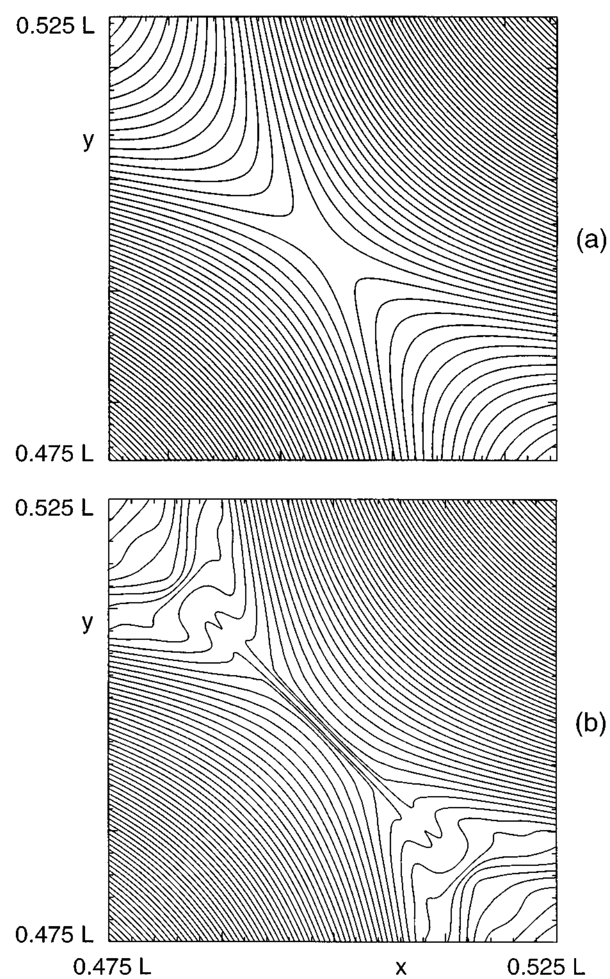

FIG. 4. Blowups of the reconnection region of the run shown in Figs. 3(a), 3(b): (a) ψ; (b) $F = \psi - d_e^2 j$.

TABLE I. Maximum reconnection rate $E_{\max}$ for seven different EMHD runs.

d_e	ν_3	$E_{\max}$
0.1	10^{-6}	1.28
0.1	10^{-8}	1.30
0.06	10^{-8}	1.27
0.06	5×10^{-10}	1.36
0.03	10^{-8}	1.42
0.03	5×10^{-10}	1.42
0.01	10^{-8}	1.53

TABLE II. Maximum reconnection rate $E_{\max}$ and time t_0 for complete coalescence for different simulation runs for incompressible ions. $E^*=Ed_i$ is the reconnection rate in Alfvén time units.

d_i	d_e	ν_3	$E_{\max}$	t_0	$E^*_{\max}$
∞	0.03	10^{-8}	1.4	1.5	-
0.4	0.03	4×10^{-10}	1.7	1.3	0.68
0.2	0.03	10^{-8}	2.5	1.0	0.5
0.2	0.015	10^{-8}	2.4	1.0	0.48
0.2	0.03	4×10^{-10}	2.4	1.0	0.48
0.1	0.015	10^{-8}	4.4	0.5	0.44
0.1	0.015	4×10^{-10}	4.4	0.55	0.44
0.05	0.0075	4×10^{-10}	6.7	0.35	0.34

The reconnection rate E is found to be independent of d_e and ν_3, which have been varied in the intervals $10^{-1}\leqslant d_e\leqslant 10^{-2}$ and $10^{-6}\leqslant \nu_3\leqslant 10^{-12}$. Table I gives the maximum values of E for seven runs. The numbers confirm that E does not depend on d_e and ν_3 (apart from the weak *increase* of $E_{\max}$ with decreasing d_e).

In the discussion of section III A we have ignored the substructures $<d_e$ in the inertia-dominated region. Instead of a bell-shaped cross-layer current profile as in resistive MHD, in the weakly collisional EMHD system the current density develops a cusp-like profile with strong gradients increasing with decreasing viscosity. As can be expected of a fluid at high Reynolds number, turbulence is generated, which is excited by the Kelvin-Helmholtz instability of the sheared electron flow. Since transverse scales and turbulence wavelengths are short compared to d_e and $\omega_e\gg j$, Eq. (19) reduces to the 2D Euler equation. Kelvin-Helmholtz instability arises, roughly speaking, if $kl_s<1$, where l_s is the scale of the velocity gradient and k the wavenumber, and $\gamma\sim v/l_s$ is a typical growth rate. In addition the aspect ratio Δ/l_s has to be sufficiently large.

Though the onset of turbulence does not increase the reconnection rate, which already in the laminar case depends only on the global configuration, its main effect is to provide a finite dissipation rate R. While for laminar flows R decreases with decreasing viscosity, R becomes independent thereof, if turbulence is generated. These and other properties of EMHD turbulence have recently been discussed in Ref. 15.

C. Effect of ion inertia

In the previous subsections we have shown analytically and numerically that the electron dynamics responsible for reconnection to occur adjusts to the outside conditions, such that the reconnection rate E does not depend on the electron physics characterized by d_e and ν_e. Hence E depends only on the ion physics, characterized by d_i and ν_i, which has been studied by numerical simulations of the incompressible Eqs. (8), (11), (16), (17).

Since it is numerically difficult to combine the most interesting case $d_i\ll 1$ with a realistic ratio $d_i/d_e=\sqrt{m_i/m_e}\sim 50$, we choose values $d_i/d_e\sim 10$, varying both d_i, $0.4\geqslant d_i\geqslant 0.05$, and d_i/d_e, $13.3\geqslant d_i/d_e\geqslant 6.6$, to obtain the relevant scaling laws. A typical state from a simulation run with $d_i=0.1$, $d_e=0.015$, $\nu_i=10^{-5}$, $\nu_e=10^{-6}$ has been shown in Fig. 1.

Table II gives the maximum reconnection rates and total reconnection times for a series of runs with different values of d_i, d_e, ν_3. Here we used again third-order diffusion operators. The numbers show that the reconnection rate is in fact independent of the electron physics given by d_e and the dissipation coefficients, but depends on the ion inertia d_i. Thus, the reconnection time is no longer linked to the whistler time scale of the flux bundles. It is therefore useful to rescale E to the Alfvén time $\tau_A=d_i\tau_w$, which facilitates the interpretation of the results. In Table II the reconnection rate $E^*=Ed_i$ in units of the Alfvén time is also displayed. We see that normalized in the conventional way the reconnection rate decreases only weakly as d_i is reduced. For the range of d_i considered the reconnection speed is therefore almost Alfvénic. Consistent with this fast reconnection rate the ion flow does not form an extended layer. In fact the ion velocity changes abruptly in a shock-like way from lower inflow to higher outflow values, a behavior reminiscent of Petschek's configuration.

The asymptotic scaling laws for $d_i\rightarrow 0$ are, however, difficult to assess from the present simulation results. It cannot be excluded that the ions form a macroscopic flow layer of width d_i giving rise to relatively slower reconnection $E^*\sim d_i$. Indeed, if the reconnection rate is sub-Alfvénic for small d_i, the analysis by Waelbroeck[19] would indicate that the external MHD solution should force a macroscopic current sheet to form. In any case in the high-β regime two-fluid theory predicts reconnection to be much faster than single fluid theory, where the Hall term is ignored.

The results of the incompressible computations are corroborated by solving the fully compressible Eqs. (8)–(13) in the case of a large background pressure p_0. (Whether this is ion pressure p_i or electron pressure does not make a noticeable difference.) To avoid excitation of shockwaves the pressure distribution in the flux tubes given by Eq. (31) is chosen such as to provide approximate equilibrium in the initial state. The ambient axial field is $B_{z0}=0$. As expected compressibility effects are negligibly small for large p_0 and the dynamics is practically identical with the incompressible behavior. Extending the compressible simulations we find that the global behavior in the high-β regime carries on to the $\beta\sim 1$ regime. This is also true in the presence of a finite ambient field $B_{z0}\sim B_\perp$, though this field destroys the symmetry of the incompressible reconnection process, as is clear from the $B_{z0}\nabla\cdot\mathbf{v}_e$ term in Eq. (9), which makes the analysis of the layer structure more difficult.

Let us briefly discuss the energy balance in the reconnection process. We find that magnetic energy is transformed mainly into ion flow energy, while the electron flow energy contribution is small. On the other hand the dissipation rate is mainly due to electron (viscous) dissipation R_e, the ion contribution R_i being small. The ratio R_i/R_e depends only weakly on the ratio of the dissipation coefficients.

IV. THE LOW-β CASE

For large axial field B_{z0}, i.e. small β, the plasma motion is again nearly incompressible as follows from Eq. (9). Similarly to p in the high-p_0 case, b in the high-B_{z0} case can no longer be determined from the original equation, since this would require knowledge of the residual value of $\nabla\cdot\mathbf{v}$, the term $B_{z0}\nabla\cdot\mathbf{v}$ being finite. Instead b is obtained by taking the divergence of the equation of motion:

$$d_i^2\nabla\cdot(\nabla\cdot\mathbf{v}_i\mathbf{v}_i)\simeq d_i^2\mathbf{v}_i\cdot\nabla\nabla\cdot\mathbf{v}_i\simeq B_{z0}\nabla^2 b-\nabla\cdot(j\nabla\psi). \tag{32}$$

The b equation, on the other hand, provides an expression for $\nabla\cdot\mathbf{v}$,

$$\nabla\cdot\mathbf{v}\simeq-\frac{1}{B_{z0}}\mathbf{B}\cdot\nabla j,$$

since the remaining terms in Eq. (9) are found to be small. Hence the inertia term in Eq. (32) is $O(B_{z0}^{-1})$, such that b is determined by the equilibrium equation, which yields

$$\frac{b}{B_y}\sim\frac{B_y}{B_{z0}}\ll 1. \tag{33}$$

Comparing this behavior with the high-β situation, where the whistler dominates characterized by Eqs. (15) and (25), we see that the whistler is suppressed by a strong axial field. Hence we can ignore the poloidal current density, ions and electrons are essentially moving together in the poloidal plane $\mathbf{v}_{e\perp}\simeq\mathbf{v}_{i\perp}\gg\mathbf{j}_\perp$, such that the dynamics is determined by the equations for the flux function ψ and the stream function φ of the incompressible plasma flow $\mathbf{v}=\mathbf{e}_z\times\nabla\varphi$, $\omega=\nabla^2\varphi$,

$$\partial_t(\psi-d_e^2\nabla^2\psi)+\mathbf{v}\cdot\nabla(\psi-d_e^2\nabla^2\psi)=-\nu_e\nabla^2\nabla^2\psi, \tag{34}$$

$$\partial_t\omega+\mathbf{v}\cdot\nabla\omega-\mathbf{B}\cdot\nabla\nabla^2\psi=\nu_i\nabla^2\omega. \tag{35}$$

This model has previously been discussed in Refs. 4 and 5. While in a high-β plasma the ion flow is confined to a layer of width d_i, in a low-β plasma imbedded in a strong axial field the ions are forced to flow in a layer of width d_e. The reconnection configuration consists of a macroscopic current sheet of length L and width d_e, leading to the scaling

$$u\sim(Ed_e)^{1/2}, \tag{36}$$

$$v\sim B_y\sim(E/d_e)^{1/2}. \tag{37}$$

Since the magnetic energy $\sim B_y^2L^2$ is finite, reconnection is rather slow,

$$E\lesssim O(d_e). \tag{38}$$

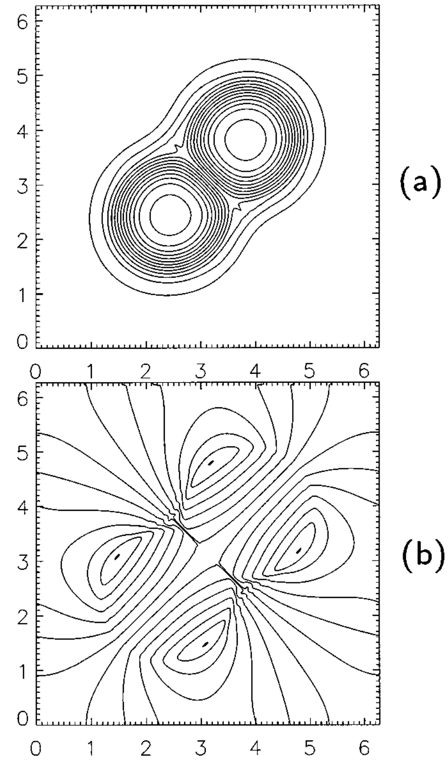

FIG. 5. Flux bundle coalescence neglecting the Hall term, Eqs. (34), (35): Contours of (a) ψ, (b) φ.

A typical state from a simulation of Eqs. (34), (35) is shown in Fig. 5. The results of simulations based on Eqs. (8)–(13) are presented in Table III to illustrate the transition from the compressible $B_{z0}\sim 1$ case to the incompressible case of large $B_{z0}\gg 1$. While for $B_{z0}=1$ the reconnection rate is independent of d_e, it strongly decreases with d_e for $B_{z0}\gg 1$ approaching the scaling $E\sim d_e$, Eq. (38). A crude estimate of the ion flow layer width δ_i gives $\delta_i/d_i\sim b/B_{y0}\sim B_{y0}/B_{z0}$, where B_{y0} is the poloidal field in front of the layer. Hence E becomes independent of B_{z0}, if $B_{z0}/B_{y0}>d_i/d_e$.

V. CONCLUSIONS

We have studied the properties of quasi-collisionless reconnection in the framework of two-fluid theory, restricted to two-dimensional geometry. In the high-β case the dynamics is controlled only by ion inertia, being independent of the electron physics, in particular electron inertia and electron viscosity. This behavior can be linked to the whistler mode, which decouples the electrons from the ions on scales

TABLE III. Maximum reconnection rate for different axial fields B_{z0}; $d_i=0.2$.

B_{z0}	$E_{\max}(d_e=0.03)$	$E_{\max}(d_e=0.015)$
1	2.51	2.54
2.5	2.25	2.25
5	1.98	1.77
10	1.38	0.86
20	1.25	0.74

$l < c/\omega_{pi}$. Since the group velocity of the whistler increases with decreasing spatial scales, the electrons form an X-point configuration with a flow converging and accelerating toward this point. This flow is only changed at scales $l \sim c/\omega_{pe}$, where the whistler mode becomes slow. The behavior is described by the equations of electron magnetohydrodynamics. We have given a self-similar solution valid for $c/\omega_{pi} > l > c/\omega_{pe}$, which can be matched to the micro-current layer around the X-point, the scaling laws of which have been derived. The configuration differs fundamentally from the macro-current sheet set up in resistive MHD reconnection. Numerical simulations show that for not too small values of $d_i = c/\omega_{pi}L$ the reconnection speed is almost Alfvénic depending only weakly on d_i. The behavior in the limit $d_i \ll 1$ is difficult to assess. It cannot be excluded that in this limit a macro-current sheet of width c/ω_{pi} is formed, giving rise to a reconnection rate $E \sim d_i$.

The results of the high-β regime carry on to $\beta \sim 1$, which is typical for plasma conditions in the solar wind and the earth's magnetotail. Though for $\beta \sim 1$ plasma compressibility is not negligible and the presence of a finite mean axial field gives rise to a more complicated nonsymmetric structure of the current layer, the global behavior is hardly changed, remaining independent of the electron dynamics.

In the case of a large axial field $B_{z0} \gg B_\perp$, however, the reconnection efficiency is strongly reduced. Since the axial field suppresses the whistler mode, electrons and ions are tightly coupled confining the ions to the narrow electron layer c/ω_{pe}. This corresponds to the model where the Hall-term, i.e. the poloidal current density, is neglected, hence $E \sim d_e$. We thus find that the large-B_{z0} case is much different from the high-β one. Though in both regimes plasma flows are nearly incompressible, assuming exact incompressibility is only correct for high β, while in the large-B_{z0} case the residual value of $\nabla \cdot \mathbf{v}$ suffices to suppress the whistler mode, drastically reducing the reconnection efficiency.

Let us emphasize again the role of the viscosities. These are important to prevent the formation of singular velocity gradients, which tend to form in the collisionless limit, velocity profiles having a cusp-like shape. The global dynamics, in particular the reconnection rate, is independent of the viscosity coefficients, if these are sufficiently small, hence the term collisionless reconnection is appropriate.

One formal limitation of the model's validity is due to the omission of Larmor radius effects. To judge these, a fully kinetic model is needed. Recent particle simulations, however, indicate that for $\beta_i \sim 1$, i.e. $\rho_i \sim d_i$ the reconnection rate is unchanged compared with the fluid results. These results will be published in a separate paper. In the opposite case of a strong axial field our 2D model does not account for the $\nabla_\parallel p_e$ effect treated in Refs. 6–8, which leads to efficient reconnection for $\rho_s > c/\omega_{pe}$, i.e. $\beta > m_e/m_i$.

[1] See, e. g., A. M. Edwards, D. J. Campbell, W. Engelhardt, H. U. Fahrbach, R. D. Gill, R. S. Granetz, S. Tsuji, B. J. D. Tubing, A. Weller, J. Wesson, and D. Zasche, Phys. Rev. Lett. **57**, 210 (1986).
[2] D. N. Baker, J. Geophys. Res. **101**, 12975 (1996)
[3] K. Shibata, Adv. Space Res. **17**, 9 (1996).
[4] J. F. Drake and R. G. Kleva, Phys. Rev. Lett. **66**, 1458 (1991).
[5] M. Ottaviani and F. Porcelli, Phys. Rev. Lett. **71**, 3802 (1993).
[6] A. Y. Aydemir, Phys. Fluids B **4**, 3469 (1992).
[7] J. F. Drake, R. G. Kleva, and F. L. Waelbroeck, Phys. Plasmas **2**, 23 (1995).
[8] B. Rogers and L. Zakharov, Phys. Plasmas **3**, 2411 (1996).
[9] M. E. Mandt, R. E. Denton, and J. F. Drake, Geophys. Res. Lett. **21**, 73 (1994).
[10] D. Biskamp, E. Schwarz, and J. F. Drake, Phys. Rev. Lett. **75**, 3850 (1995)
[11] See, e.g., D. Biskamp, Phys. Rep. **237**, 181 (1994).
[12] A. S. Kinsep, K. V. Chukbar, and V. V. Yankov, in *Review of Plasma Physics* (Consultants Bureau, New York, 1990), Vol. 16.
[13] S. V. Bulanov, F. Pegoraro, and A. S. Sakharov, Phys. Fluids B **4**, 2499 (1992).
[14] J. F. Drake, R. G. Kleva, and M. E. Mandt, Phys. Rev. Lett. **73**, 1251 (1994).
[15] D. Biskamp, E. Schwarz, and J. F. Drake, Phys. Rev. Lett. **76**, 1264 (1996).
[16] D. Biskamp, Phys. Fluids **29**, 1520 (1986).
[17] See, e.g., D. Biskamp, *Nonlinear Magnetohydrodynamics* (Cambridge University Press, Cambridge, 1993), p. 147.
[18] D. Biskamp and H. Welter, Phys. Fluids B **1**, 1964 (1989).
[19] F. L. Waelbroeck, Phys. Fluids B **1**, 2372 (1989).